Brazilian Journal
of Chemical
Engineering

ISSN 0104-6632
Printed in Brazil
www.abeq.org.br/bjche

Vol. 34, No. 01, pp. 295 - 306, January - March, 2017
dx.doi.org/10.1590/0104-6632.20170341s20160120

SYNTHESIS OF 2,6-DIMETHYLNAPHTHALENE OVER SAPO-11, SAPO-5 AND MORDENITE MOLECULAR SIEVES

Xiaoxiao Wang[1*], Zhenmin Liu[1], Xianxian Wei[2], Fang Guo[3], Peng Li[1] and Shaoqing Guo[2*]

[1]Taiyuan University of Science and Technology, School of Chemical and Biological Engineering, Taiyuan 030021, PR China.
Phone: + (86) 03512307368
[*]E-mail: wang5203264@sina.com
[2]Taiyuan University of Science and Technology, College of Environment and Safety, Taiyuan 030024, PR China.
Phone: +(86) 03512307368
[*]E-mail: guosq@sxicc.ac.cn
[3]Jin Zhong University, College of Chemistry and Chemical Engineering, Yuci 030619, PR China.

(Submitted: February 22, 2016 ; Revised: April 26, 2016 ; Accepted: June 19, 2016)

Abstract - Shape-selective methylation of naphthalene over SAPO-11, SAPO-5 and mordenite molecular sieves were carried out in a fixed-bed flow reactor under atmospheric pressure. Methanol and mesitylene were used as methylation and solvent agents. The experiment results showed that SAPO-11 exhibited higher stability, higher selectivity of 2,6-dimethylnaphthalene (2,6-DMN) and higher 2,6-/2,7-DMN ratio than SAPO-5 and mordenite molecular sieves. The catalytic performances for the methylation of naphthalene were mainly related to the pore structure of the catalysts. The comparison of the spent SAPO- 11 with fresh SAPO-11 suggested that structure collapse of the SAPO-11 by dealumination was occurred during the methylation of naphthalene with methanol, which may have been caused by high temperature steam from water produced in the reaction or by high temperature methanol vapor.
Keywords: Molecular sieves; Naphthalene methylation with methanol; Deactivation.

INTRODUCTION

2,6-Dialkylnaphthalene (2,6-DKN) is an important product in industry, which can be oxidized to 2,6-naphthalene dicarboxylic acid (2,6-NDA) and then to prepare the commercially valuable polymer of poly(ethylene naphthalene dicarboxylate) (PEN). Compared with poly(ethylene terephthalate) (PET), in addition to its excellent properties as a gas barrier, PEN has good thermal and chemical stability as well as mechanical properties, leading to its wide application in electronics components, insulation material, food containers, aviation, and so on (Song *et al*., 1993; Tsutsui *et al*., 2004; Wu *et al*., 2010; Wu *et al*., 2015). Highly regioselective synthesis of 2,6-DKN can be achieved over different molecular sieve catalysts using various alkylating agents and solvents (Brzozowski *et al*., 2012; Liu *et al*., 1997; Smith *et al*., 2000; Smith *et al*., 2003; Smith *et al*., 2012; Song *et al*., 2000; Sugi *et al*., 2008). Liu *et al*. (1997) reported that the alkylation of naphthalene with t-butanol should be both practical and attractive not only because of the high activity, but also due to the easy separation of the desired product from the reaction mixtures by crystallization. Smith *et al*. (2000) surveyed the dialkylation of naphthalene over a dealuminated mordenite molecular sieve using tert-butanol as an alkylating agent. The experimental

*To whom correspondence should be addressed

results showed that a 60% yield of 2,6-di-tert-butylnaphthalene was obtained with a 2,6/2,7-ratio of over 50. Sugi *et al*. (2008) reported that the channels of molecular sieves with three dimensional pore-system were too large to differentiate 2,6-DAN from other β,β-DAN by restriction of their transition states in the channels even with bulky alkylating agents of 1-butene and 2-methylpropene.

Among 2,6-DKNs, 2,6-dimethylnaphthalene (2,6-DMN) is regarded as the most suitable raw material for the synthesis of PEN because no carbon atoms of 2,6-DMN are lost in the oxidation reaction and 2,6-DMN can be oxidized easily compared with other 2,6-DKNs (Pu *et al*., 1996). At present, 2,6-DMN is mainly produced by BP-Amoco through a four-step process from o-xylene and butadiene, but the process is quite complex (Lillwitz *et al*., 2001). In order to establish a simple and "green" synthesis route of 2,6-DMN with fewer reaction steps and less reaction waste, it is desirable to methylate naphthalene to 2,6-DMN directly over a shape-selective molecular sieve catalyst.

In recent years, methylation of naphthalene over molecular sieve catalysts to synthesize 2,6-DMN was reported by several research groups. As a result, there were great differences in the catalytic activity and selectivity among these molecular sieves (Fraenkel *et al*., 1986; Park *et al*., 2002; Jin *et al*., 2006; Yoo *et al*., 2002; Jin *et al*., 2006; Wu *et al*., 2010). For example, Fraenkel *et al*. (1986) first investigated the methylation of naphthalene with methanol over ZSM-5, mordenite and HY molecular sieves, and found that the medium pore size ZSM-5 showed a high product selectivity and moderate activity, while the large pore size molecular sieves, HY and mordenite, providing enough space for multiple reactions, would lead to a lower product selectivity and a higher activity. Park *et al*. (2002) reported that the selectivity for 2,6+2,7-DMN was only 16% using MCM-22 as catalyst after 1 hour time-on-stream (TOS). Yoo *et al*. (2002) reported that the high stability of ZSM-12 molecular sieves during the methylation was because ZSM-12 possessed one dimensional non-interpenetrating channels which behaved as "perfect tubes" and did not lead to the accumulation of coke precursors. Jin *et al*. (2006) reported that Zr/(Al)ZSM-5 could improve the selectivity of 2,6-DMN and the stability of the catalyst. They attributed it to the weakening of the acid strength and the enlargement of the pore dimensions because of the part incorporation of Zr in the framework instead of Al. Wu *et al*. (2010) concluded that the small dimensions of zeolites crystals and the advanced mesoporosity were the general reasons for the remarkable catalytic action of MTW zeolites in naphthalene methylation. Among these molecular sieves, SAPO-11 molecular sieve has been proved to show high catalytic performances in the methylation of naphthalene with methanol (Liu *et al*., 2013; Wang *et al*., 2012; Wang *et al*., 2013; Wang *et al*., 2015). First of all, SAPO-11 is a one-dimensional pore zeolite with pore opening of 0.39 nm × 0.64 nm (Liu *et al*., 2015; Wu *et al*., 2015; Zhang *et al*., 2007), which is between the pore size of large-pore molecular sieves and the pore size of medium-pore molecular sieves, making it an interesting material for catalytic cracking, reforming and alkylation (Subramanian *et al*., 1997; Prakash *et al*., 1996; Han *et al*., 2014; Liu *et al*., 1991; Rabaev *et al*., 2015; Tian *et al*., 2014; Wang *et al*., 2015). Similar to ZSM-12, SAPO-11 also possesses one dimensional and non-intersecting channels (Zhang *et al*., 2010), which shows excellent resistance to deactivation by carbonaceous deposition.

Based on these reports, it is concluded that the catalytic activity for the methylation of naphthalene has relation with the acidity and the structure of molecular sieves. However, the effect of the acidity and the structure of molecular sieves on the naphthalene methylation with methanol have not been understood clearly, which hinders the development of a commercial catalyst for naphthalene methylation. In addition, the research on deactivation of SAPO-11 molecular sieve during methylation of naphthalene with methanol has not been reported. Meanwhile, there are few studies about the methylation of naphthalene with methanol over SAPO-5 molecular sieve so far.

In the present work, SAPO-11, SAPO-5 and mordenite were evaluated for the methylation of naphthalene with methanol, respectively. And they were investigated in detail by using ammonia temperature programmed desorption (NH_3-TPD), infrared spectroscopy with pyridine adsorption (Py-IR) and N_2 adsorption techniques in order to study the impact of the pore structure and acidity of molecular sieves on catalytic performance in the methylation of naphthalene with methanol. In addition, the fresh and the spent SAPO-11 molecular sieves have been characterized by different characterization methods to analyze the cause of deactivation of the SAPO-11.

EXPERIMENTAL

Catalyst Preparation

Mordenite was obtained from the Catalyst Plant of Nankai University. The acidic form of the molecu-

lar sieve was prepared by ion-exchange with aqueous NH_4NO_3 solution and then calcination at 550 °C for 2 h in air.

SAPO-5 and SAPO-11 were synthesized hydrothermally. Pseudoboehmite (75 wt% Al_2O_3), orthophosphoric acid (85% H_3PO_4) and silica sol (30 wt% SiO_2) were used as source of Al, P and Si. Di-n-propylamine (DPA) was used as the template.

SAPO-11 was synthesized by hydrothermally crystallizing a sol-gel mixture with a composition of $1.0Al_2O_3$:$1.0P_2O_5$:$0.6SiO_2$:1.2DPA:$49H_2O$ (Blasco *et al*., 2006). The final crystallization temperature of 180 °C and crystallization time of 20-28 h were employed. The products were washed with distilled water, then dried at 120 °C for 5 h and calcined at 600 °C for 4 h.

SAPO-5 was synthesized by a hydrothermal method from a gel molar composition of $1.0Al_2O_3$: $1.1P_2O_5$:$0.66SiO_2$:1.6DPA:$40H_2O$. The gel mixture was transferred into a stainless steel autoclave, heated in an oven at 200 °C for 6 h, and subsequently at 300 °C for 9 h. The product thus obtained was washed, dried at 120 °C for 6 h, and calcined in air at 550 °C for 24 h to remove the template completely.

Catalyst Characterization

X-ray powder diffraction (XRD) analysis was performed on RigakuD/maxrB X-ray diffractometer. Diffraction patterns were recorded with Cu Ka radiation at 40 kV and 100 mA in the scan range between 5^o and 50^o to identify the phase structure of the catalyst.

The morphologies of the samples were examined by Hitachi S-4800 scanning electron microscopy (SEM).

The textural properties of the samples were derived from N_2 adsorption-desorption measurement on Micromeritics Tristar 3000. In each case, the sample was outgassed under vacuum at 300 °C for 3 h before N_2 adsorption.

The acidity of the samples was examined by temperature-programmed desorption of ammonia (NH_3-TPD) techniques carried out by a flow system with a thermal conductivity detector. All samples were preheated from room temperature to 500 °C in an argon flow and kept at 500 °C for 1 h, which was followed by NH_3 saturation in a flowing NH_3/Ar stream at 40 °C for 5 min. Evacuation at 40 °C for 40 min was carried out to remove physically adsorbed NH_3 then the catalyst was heated to 600 °C at a linear rate of 10 °C·min^{-1}, and the detector signal of NH_3 was recorded.

The acid sites of the catalyst samples were characterized by FT-IR (EQUINOX55) spectroscopy with chemisorbed pyridine.

The thermogravimetric analysis and differential thermal analysis (TG-DTA) were recorded on a Rigaku Thermo plus Evo TG 8120 instrument at a heating rate of 10 °C·min^{-1} in air with a flow rate of 30 ml·min^{-1}.

The total (bulk) Si and Al contents in the catalysts were determined by an Inductive Couple Plasma (ICP) emisson spectrometer (Thermo ICAP6300). The SAPO-11 catalyst was subjected to themogravimetric analysis both before reaction (fresh) and after reaction (spent).

Catalytic Evaluation

The experiments were performed in a fixed-bed continuous-flow reactor equipped with 20 mm diameter and 600 mm length stainless steel tube. 2.5 g of 20-40 mesh molecular sieve catalysts were loaded in the reaction tube. After preheating, the reaction mixture including naphthalene, methanol and mesitylene (solvent) in a molar ratio of 1:5:3.5 was fed into the reactor by a quantity measuring pump under the pressure kept by N_2. The weight hourly space velocity (WHSV) of naphthalene was 0.19 h^{-1} in all experiments, and the reactive temperature was 350 °C. Reaction products were analyzed by gas chromatography (GC9560) with a Beta-Dex120 capillary column.

The naphthalene conversion was calculated as follows:

$$\text{naphthalene conv.}(\%) = \left(\frac{n_{N,0} - n_N}{n_{N,0}} \right) \times 100\%$$

where $n_{N,0}$ and n_N are the molar percentage of naphthalene before and after the reaction. Product distribution includes the corresponding molar percentages of ethylnaphthalene (EN), methylnaphthalene (MN), dimethylnaphthalene (DMN) and trimethylnaphthalene (TMN) in the total product mixture. The selectivity of 2,6-DMN and 2,7-DMN is the corresponding molar percentage in the sum of all DMN isomers, respectively. 2,6-/2,7-DMN stands for the molar ratio of 2,6-DMN to 2,7-DMN. The 2,6-DMN yield was calculated by the following equation.

2,6-DMN yield (%) = (naphthalene conversion × 2,6-DMN distribution) /100%.

RESULTS AND DISCUSSION

Characterization of Catalysts

XRD patterns of as-synthesized SAPO-5 and SAPO-11 samples presented in Figure 1 show the presence of highly crystalline SAPO phases and no impurity phases are detected (see Figure 1). The characteristic peaks of the SAPO-11 phase (i.e. 2θ = 8. 15°, 9. 40°, 13. 20°, 15. 57°) are observed and are identical to those reported for SAPO-11 in the literature (Lok *et al*., 1984). Also the positions of the lines of the SAPO-5 are identical to those reported for SAPO-5 (Wei *et al*., 2015; Zhu *et al*., 2016). It is a well-crystallized sphere-shaped material as determined by the SEM studies (see Figure 2).

According to the reference materials (Zhang *et al*., 2007; Chao *et al*., 2000; Bandyopadhyay *et al*., 2002), the physicochemical properties of the investigated molecular sieves are summarized in Table 1. The BET surface area and the pore volume of SAPO-11, SAPO-5 and Mordenite molecular sieves are determined by N_2 adsorption-desorption measurement. As observed in Table 1, the surface area and the pore volume of the investigated molecular sieves decrease in the order of Mordenite > SAPO-5 > SAPO-11.

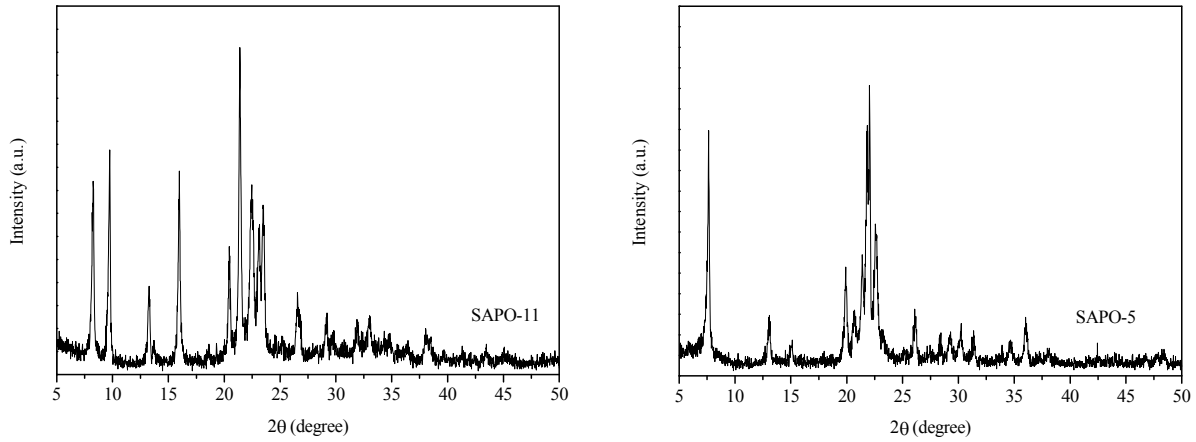

Figure 1: XRD Patterns of SAPO-11 sample and SAPO-5 sample.

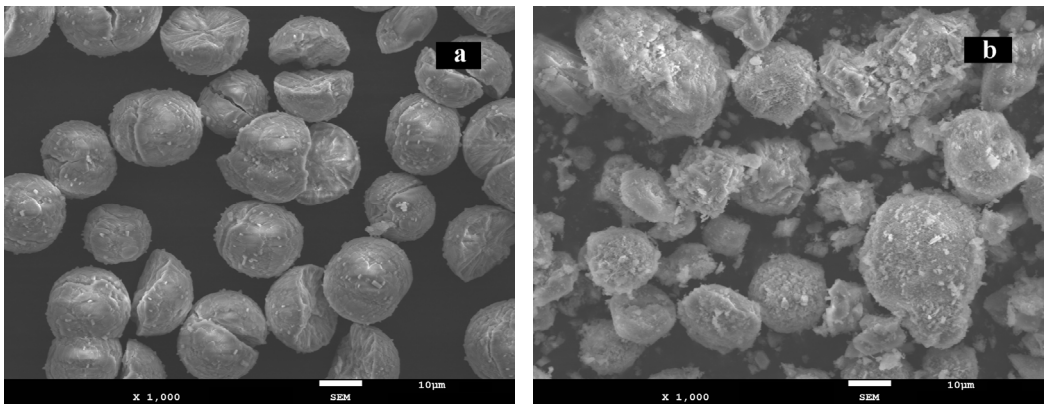

Figure 2: SEM images of SAPO-11 sample (a) and SAPO-5 sample (b).

Table 1: Physicochemical properties of different molecular sieves.

Molecular sieves	SiO_2/Al_2O_3	Topology①	Channel structure②	Pore Opening /nm③	BET surface area/ (m^2/g)	Pore volume/(cm^3/g)
Mordenite	25	MOR	Unidimensional	0.65×0.70 (001)	318	0.176
SAPO-5	-	AFI	Unidimensional	0.73×0.73 (001)	238	0.160
SAPO-11	-	AEL	Unidimensional	0.39×0.64 (001)	216	0.145

Zhang *et al*., 2007;②Chao *et al*., 2000;③Bandyopadhyay *et al*., 2002

The acidic properties are usually evaluated by NH_3-TPD, and the profiles can be differentiated both in the integral area of the profiles and in the shift of peak temperature. The former corresponds to the amount of acid sites, and the latter indicates the strength of the acid sites. The NH_3-TPD profiles of different catalyst samples illustrated in Figure 3 present three ammonia desorption peaks at ca. 210 °C, 300 °C and 510 °C, corresponding to a weak acid site, a medium strong acid site and a strong acid site. The acidity values of different molecular sieve catalysts are shown in Table 2. From Figure 3 and Table 2, it can been seen that the total acidity of the molecular sieves and the acid strength of their acidic sites both decrease in the order of Mordenite > SAPO-11 > SAPO-5.

Pyridine-IR is used to further evaluate the type (Lewis and Bronsted) of acid sites for all the samples. The Bronsted acid sites of the investigated molecular sieves will protonate pyridine, forming the pyridinium ion, which has a characteristic ring vibrational frequency at 1540 cm^{-1}. Lewis aluminum, being an electron-pair acceptor, can bind pyridine in a covalent fashion, giving rise to a vibrational band at 1450 cm^{-1}. The relative amounts of Bronsted and Lewis acid sites can be estimated by integration of these two bands after correction for differences in oscillator strengths (Harris *et al*., 2016; Nieminen *et al*., 2004). The concentration of Bronsted and Lewis acid sites after pyridine desorption at 200 °C and 400 °C are presented in Table 3. At any desorption temperature, the density of Bronsted acid sites of these samples decreases in the order of Mordenite > SAPO-11 > SAPO-5, indicating that the strong acid sites of these samples decreases in the same order, which is in agreement with the results of NH_3-TPD shown in Figure 3. Meanwhile, Bronsted acid sites are predominant for all the investigated molecular sieves, but the ratio of Bronsted acid sites to Lewis acid sites varies among different molecular sieves. This may be due mainly to the fact that the acidic sites of molecular sieves, i.e., aluminum species of molecular sieves-framework Al and external-framework Al, change with the synthetic methods and conditions (Zhu *et al*., 2006).

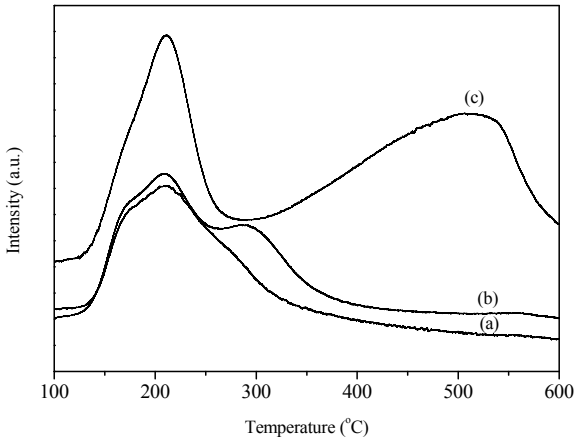

Figure 3: NH_3-TPD profiles of samples SAPO-5 (a), SAPO-11(b), Mordenite (c).

Table 2: Acidity values of different molecular sieves.

Sample	weak acid sites		Medium strong acid sites		strong acid sites		The total acid amount / (mmol g^{-1})
	Peak temperature / °C	The acid amount / (mmol g^{-1})	Peak temperature / °C	The acid amount / (mmol g^{-1})	Peak temperature / °C	The acid amount / (mmol g^{-1})	
SAPO-5	210	0.55	0	0	0	0	0.55
SAPO-11	210	0.47	288	0.28	0	0	0.76
Mordenite	213	0.68	0	0	516	11.2	11.88

Table 3: Bronsted acid sites and Lewis acid sites of molecular sieves spectra of absorbed pyridine[a].

Samples	Bronsted acid sites		Lewis acid sites		Total acid sites	
	200 (°C)	400 (°C)	200 (°C)	400 (°C)	200 (°C)	400 (°C)
Mordenite	23.25	18.12	10.2	6.56	33.45	24.68
SAPO-11	11.76	11.46	2.20	0.58	13.96	12.04
SAPO-5	11.2	10.2	1.90	0.43	13.1	10.63

Catalytic Activity in the Methylation of Naphthalene

The catalytic performances of the investigated molecular sieves with 1h of TOS are listed in Table 4. It can be seen that 1,8-DMN is not detected for all the molecular sieves, probably due to steric repulsion. Among all the molecular sieves in the present study, Mordenite exhibits relatively high naphthalene conversion compared with the other molecular sieves. SAPO-11 exhibits the highest selectivity for DMN, i.e. 52.8% with the very high 2,6-/2,7-DMN ratio of 1.46 for 1 h of TOS. The 2,6-DMN yield decreases in the order of SAPO-11 > Mordenite > SAPO-5.

Table 4: Comparison of catalytic performance of different molecular sieves in the methylation of naphthalene.

	Mordenite	SAPO-11	SAPO-5
Naphthalene onv(%)	**60.2**	**55.2**	**26.1**
Product distribution (mol%)			
EN	3.50	0	1.07
MN	40.1	43.7	51.8
DMN	36.3	52.8	39.7
TMN	20.1	3.5	7.43
DMN distribution (mol%)			
2,6-DMN	22.6	23.9	21.30
2,7-DMN	20.5	16.4	21.4
1,7-DMN	20.0	13.4	20.1
1,3-DMN	6.0	7.93	6.81
1,6-DMN	18.1	12.5	15.89
2,3-DMN	5.6	8.33	2.90
1,4-DMN	2.4	4.51	1.80
1,5-DMN	1.7	9.43	9.8
1,2-DMN	3.1	3.60	0
1,8-DMN	0	0	0
2,6-/2,7-DMN	1.10	1.46	0.99
2,6-DMN yield	4.94	6.96	2.73

Reaction conditions: Temperature = 350 °C, Pressure = 0.1MPa, WHSV= 0.19h^{-1},
naphthalene:methanol:mesitylene = 1:5:3.5 (molar ratio), TOS = 1h.
Product distribution includes the corresponding molar percentages of EN (ethylnaphthalene), MN (methylnaphthalene), DMN (dimethylnaphthalene) and TMN (trimethylnaphthalene) in the total product mixture.

The catalytic conversion of the investigated molecular sieves is compared in Figure 4 shows that mordenite presents the highest conversion of naphthalene (60.2%) at 1h of TOS. In contrast, SAPO-11 shows the highest conversion of naphthalene (60.2%) at 6 h of TOS, and the conversion of naphthalene for SAPO-5 is the lowest in the reaction time. Meanwhile, mordenite and SAPO-5 show initially the highest conversion of naphthalene and the lowest conversion of naphthalene, respectively, which may be related to their acidity. As shown in Figure 3 and Table 2, mordenite and SAPO-5 exhibit the highest acidity and lowest acidity, respectively, leading to the initial activity of mordenite and SAPO-5 molecular sieves. In additon, Table 3 shows that mordenite has the most Bronsted acid sites and SAPO-5 possesses the least Bronsted acid sites, implying that the Bronsted acid sites probably be active sites in the methylation of naphthalene with methanol. However, their relatively low stability may be caused by the deposition of carbonaceous material ("coke") in the pores or the breakdown of the structure of the molecular sieves. The smaller pores of SAPO-11 may restrain the formation of coke, leading to somewhat greater stability.

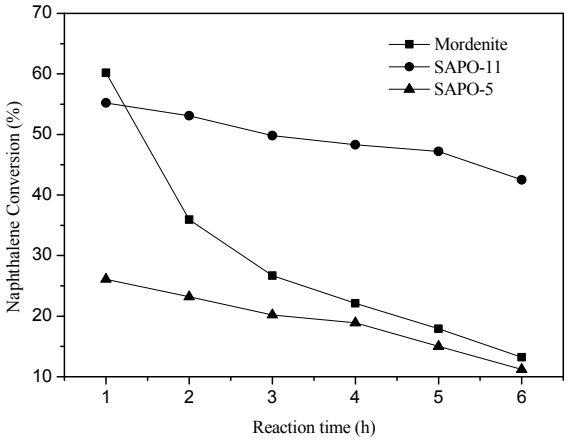

Figure 4: The conversion of naphthalene comparison of different molecular sieves.
Reaction conditions: Temperature = 350 °C, Pressure = 0.1 MPa, WHSV= 0.19 h^{-1},
naphthalene:methanol:mesitylene = 1:5:3.5 (molar ratio), TOS = 6 h.

The 2,6-/2,7-DMN ratios for the three molecular sieves are shown in Figure 5. The 2,6-/2,7-DMN ratio is very important in the purification of 2,6-DMN. It is very hard to separate them when the 2,6-/2,7-DMN ratio is less than or equal to 0.7 due to the formation of the eutectic mixture. A higher 2,6-/2,7-DMN ratio can facilitate the subsequent separation of 2,6- and 2,7-DMN mixture. When the 2,6-/2,7-DMN is more than 1.4, 2,6-DMN can be separated more easily from the eutectic mixture. As shown in Figure 5, the ratio of 2,6-/2,7-DMN on the SAPO-11 is always the highest among the investigated molecular sieves (see Table 4). However, the 2,6-/2,7-DMN ratio for the investigated molecular sieves are not associated with the acidity of the molecular sieves shown in Figure 3 and Table 2. Therefore, the 2,6-/2,7-DMN ratio is probably related to the differences in pore structure of the molecular sieves. Fang *et al*. (2006) calculated that 2,6-DMN is somewhat larger than 2,7-DMN in molecular dimension and suffers

more diffusion resistance than 2,7-DMN does during the diffusion process. Mordenite and SAPO-5, with nominal pore openings of 0.70 nm and 0.73 nm, respectively, are not expected to be very selective in the methylation of naphthalene because their channels are wide enough to accommodate the formation and diffusion of both 2,6- and 2,7-DMN molecules. SAPO-11, however, possesses a pore opening (0.39 nm×0.64 nm), which is comparable with the kinetic diameter of the naphthalene molecule (0.62 nm) and its β-methylation products (at least 0.62 nm), making it more discerning for the formation and diffusion of the 2,6- and 2,7-DMN products. Therefore, the 2,6-/2,7- DMN ratio over SAPO-11 is mainly ascribed to its specific pore structure.

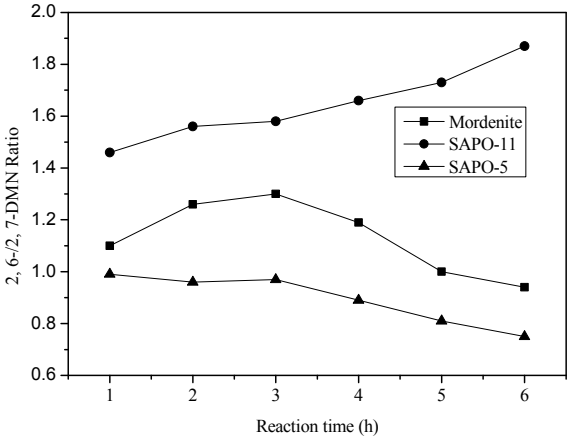

Figure 5: Effect of different molecular sieves on molar ratio of 2, 6- to 2, 7-DMN
Reaction conditions: Temperature = 350 °C, Pressure = 0.1 MPa, WHSV= 0.19 h^{-1},
naphthalene:methanol:mesitylene = 1:5:3.5 (molar ratio), TOS = 6 h.

Figure 6 shows the 2,6-DMN yield with 1-6 h of TOS on different molecular sieve catalysts. It can be seen that SAPO-11 exhibits the highest 2,6-DMN yield compared with the other molecular sieve catalysts.

All these findings prove that the relatively good catalytic performance of SAPO-11 for the methylation of naphthalene with methanol is mainly related to the catalyst's pore structure and SAPO-11 is the most promising of the catalysts tried for the methylation of naphthalene because of its suitable pore structure, which favors the formation and/or diffusion of the 2,6-DMN product over the 2,7-isomer.

Characterization of the Spent Catalyst

To further analyze the cause of deactivation of SAPO-11, the spent SAPO-11 catalyst (6 hour reaction time) was investigated in comparison with the fresh SAPO-11.

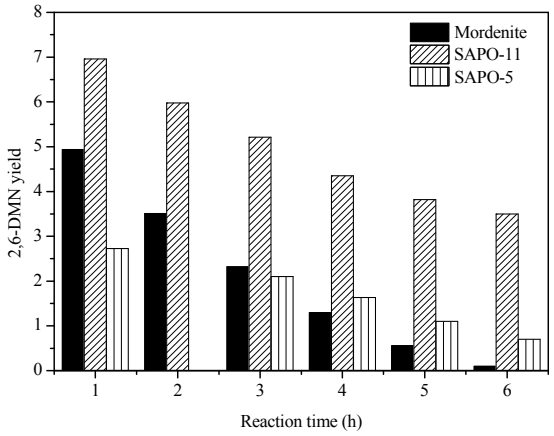

Figure 6: The 2,6-DMN yield over the investigated molecular sieves.
Reaction conditions: Temperature = 350 °C, Pressure = 0.1 MPa, WHSV= 0.19 h^{-1},
naphthalene:methanol:mesitylene = 1:5:3.5 (molar ratio), TOS = 6 h.

XRD Characterization

The XRD patterns of the fresh and the spent SAPO-11 are shown in Figure 7. The spent SAPO-11 still retains the structure of AEL (aluminophosphate eleven) type material. However, the peak strength of the spent SAPO-11 obviously decreases compared with the fresh SAPO-11 catalyst, which indicates that the crystal structure of the catalyst is severely damaged.

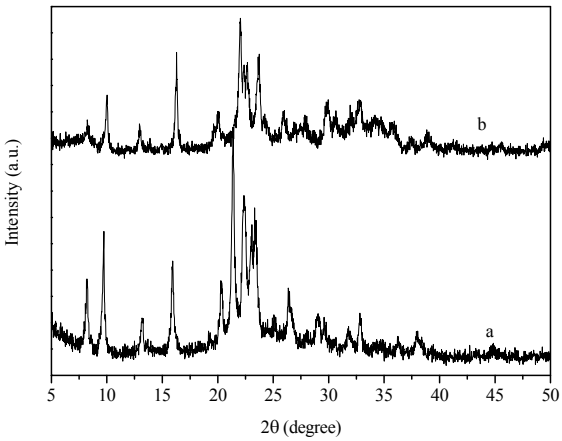

Figure 7: XRD patterns of the fresh SAPO-11 (a) and the spent SAPO-11(b).

SEM Characterization

The SEM micrographs of the fresh and the spent SAPO-11 catalysts are presented in Figure 8. Compared with the fresh SAPO-11, the SEM micrograph of the spent SAPO-11 changes dramatically. It shows that the spherical particles disappear and are replaced

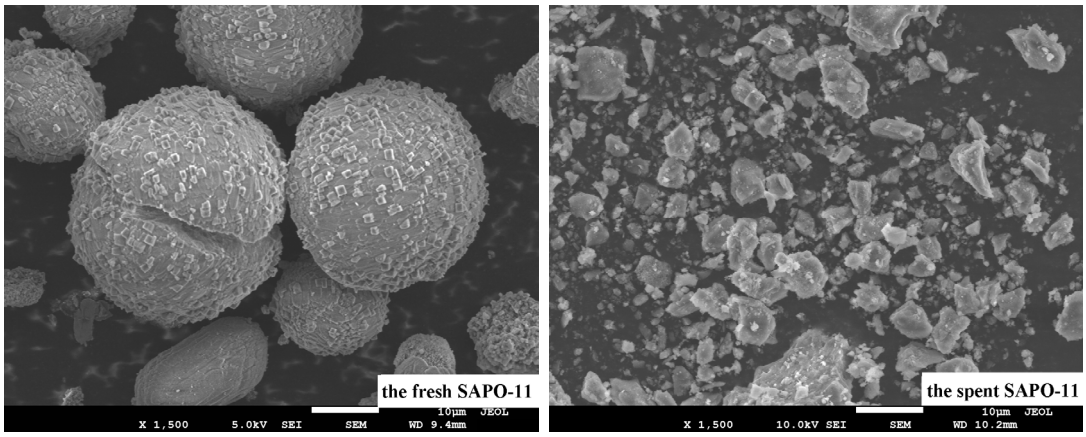

Figure 8: SEM images of the fresh and the spent SAPO-11.

by irregular particles after the reaction, which is in agreement with the results of the XRD shown in Figure 7.

ICP Characterization

The SiO_2/Al_2O_3 ratio of the fresh and the spent SAPO-11 detected by ICP are shown in Table 5. It shows that the SiO_2/Al_2O_3 ratio of the spent SAPO-11 increases compared with that of the fresh SAPO-11. That would indicate that the content of Al_2O_3 of SAPO-11 decreases after the end of reaction.

Table 5: ICP results of the fresh and the spent SAPO-11.

Sample	n(SiO_2/Al_2O_3)
fresh SAPO-11	0.53
spent SAPO-11	0.68

Pore Structure Characterization

The pore characteristics of the fresh and the spent SAPO-11 catalysts were studied by the N_2 adsorption-desorption technique, and the results of S_{BET} and V_{pore} results are listed in Table 6. The S_{BET} of 215 m^2 g^{-1} and the V_{pore} of 0.145 cm^3 g^{-1} on the fresh SAPO-11 sample decrease to 121 m^2 g^{-1} and 0.091 cm^3 g^{-1} on the spent SAPO-11 sample after the reaction, respectively.

Table 6: BET Surface area and pore volume of the fresh and the spent SAPO-11.

Sample	BET Surface area / (m^2 g^{-1})	Pore volume / (cm^3 g^{-1})
fresh SAPO-11	215	0.145
spent SAPO-11	121	0.091

The N_2 adsorption-desorption isotherms of the fresh and the spent SAPO-11 catalysts are shown in Figure 9. The typical N_2 adsorption-desorption isotherms of the SAPO-11 samples are of the type IV isotherm according to the IUPAC classification (Sing *et al*., 1985). A hysteresis between adsorption and desorption branches can be observed at medium relative pressure (0.45-1.0) for all the samples, which demonstrates the presence of a large number of secondary mesopores. However, the N_2 adsorption-desorption isotherms of the spent SAPO-11 catalyst is smaller than that of the fresh SAPO-11 catalyst.

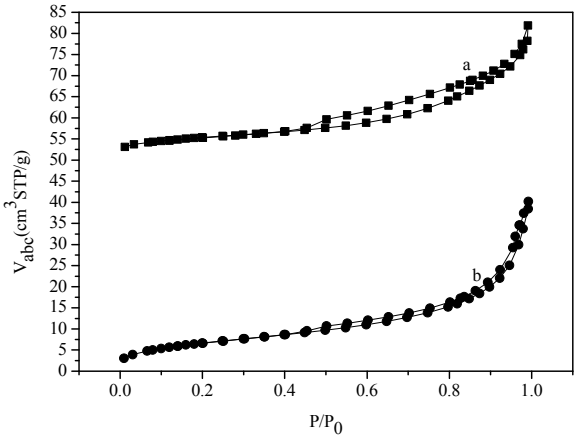

Figure 9: N_2 adsorption-desorption isotherms of the fresh (a) and the spent SAPO-11(b).

Figure 10 shows the micropores and secondary mesopores size distributions of the fresh and the spent SAPO-11 catalysts. Generally speaking, the secondary mesopores probably result from SAPO-11 microcrystals piled up during the synthesis process. As seen in Figure 10, the fresh SAPO-11 catalyst has

broader micropores size distributions and secondary mesopores size distributions than the spent SAPO-11 catalyst. From the above characterization results, we speculate that deactivation of the SAPO-11 is mainly due to the breakdown of the structure caused by dealumination (Lucas *et al*., 2009).

Thermogravimetric (TG) Analysis

The TG analysis was performed to investigate the coke deposition on the fresh and the spent SAPO-11 catalyst. The weight loss in 50-250 °C shown in Figure 11 and Figure 12 is attributed to the physically adsorbed water in the porous materials (Garces *et al*., 1988). The weight loss in 250-480 °C shown in Figure 11 is attributed to the volatilization of residual template. The weight loss in 480-800 °C in Figure 11 and the weight loss in 250-800 °C in Figure 12 are attributed to the coke deposition, which may block the active sites in the catalyst (Wang *et al*., 2011). The amount of coke deposition over the fresh SAPO-11 is 0.613% (see Figure 12), and the amount of coke deposition over the spent SAPO-11 only slightly increases to 1.64% (see Figure 12), which indicates that there is not much coke deposition caused by the acidity of SAPO-11 catalyst during the reaction process.

Acidity Characterization

The differences of the acid amount and the acid strength between the fresh and the spent SAPO-11 catalysts can be shown in Figure 13 by the NH_3-TPD profiles. Compared with the fresh SAPO-11 catalyst, the acid amount and the acid strength of the spent SAPO-11 catalyst decrease slightly.

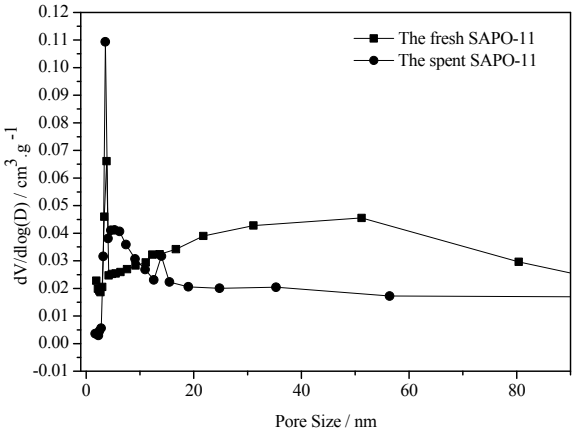

Figure 10: Pore size distributions of the fresh and the spent SAPO-11.

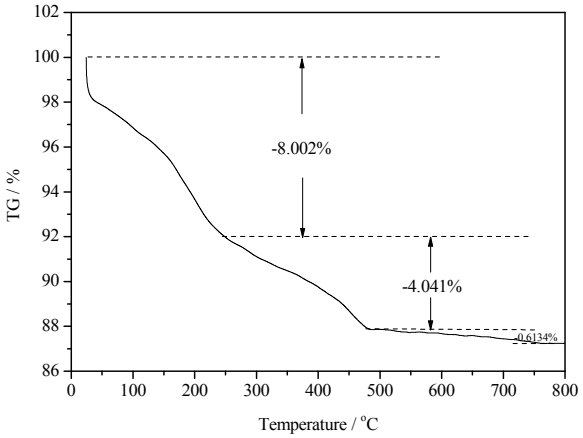

Figure 11: TG curve of weight loss of the fresh SAPO-11.

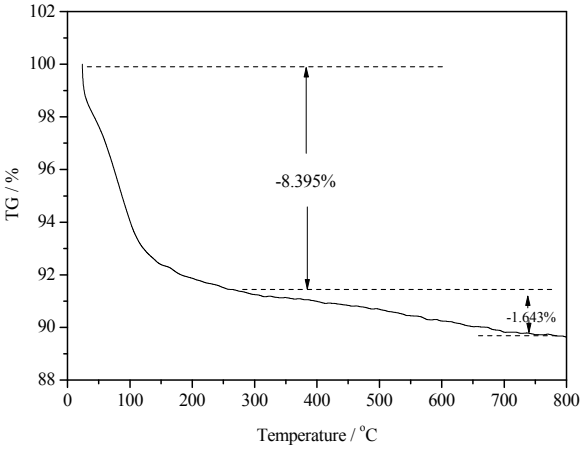

Figure 12: TG curve of weight loss of the spent SAPO-11.

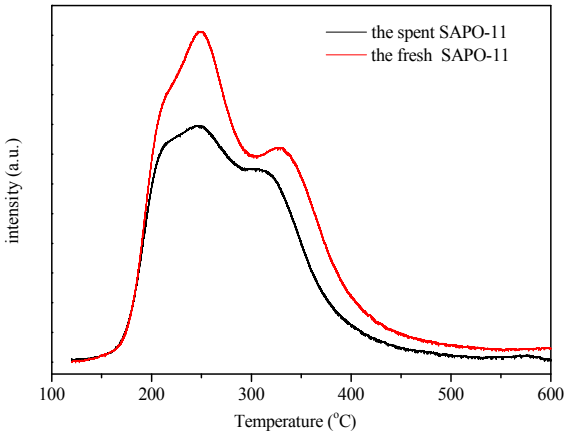

Figure 13: NH_3-TPD results of the fresh and the spent SAPO-11.

Based on the thermal gravimetric analysis and the acidity characterization, it can be inferred that the deactivation of SAPO-11 molecular sieves is not because of the coke deposition. According to the value of n(SiO_2/Al_2O_3) by ICP characterization, the deactivation of SAPO-11 is possibly because water is generated during the methylation of naphthalene with methanol, leading to the structure collapse by dealumination of the catalyst by high temperature steam or even by the methanol itself.

CONCLUSION

In summary, the catalytic activities for the methylation of naphthalene were mainly related to the pore structure of the molecular sieves catalysts and the experimental results showed that SAPO-11 exhibited higher catalytic performance than Mordenite and SAPO-5. In addition, the spent SAPO-11 was investigated in comparison with the fresh SAPO-11, which indicated that the structure of SAPO-11 had collapsed due to dealumination, probably by high temperature steam resulting from water formed in the reaction or by high temperature methanol vapor, thus resulting in the deactivation of the catalyst.

ACKNOWLEDGMENTS

This work was supported by Startup Project of Dr. of School of Chemical and Biological Engineering, Taiyuan University of Science and Technology.

REFERENCES

Bandyopadhyay, M., Bandyopadhyay, R., Tawada, S., Kubota, Y., Sugi, Y., Catalytic performance of silicoaluminophosphate (SAPO) molecular sieves in the isopropylation of biphenyl. Applied Catalysis, A: General, 225, 51-62 (2002).

Blasco, T., Chica, A., Corma, A., Murphy, W. J., Agúndez-Rodríguez, J., Pérez-Pariente, J., Changing the Si distribution in SAPO-11 by synthesis with surfactants improves the hydroisomerization/dewaxing properties. Journal of Catalysis, 242, 153-161 (2006).

Brzozowski, R., Buijs, W., Shape-selective synthesis of 2,6-diisopropylnaphthalene on H-mordenite catalysts. Journal of Catalysis, 292, 181-187 (2012).

Chao, K. J., Lin, C. C., Lin, C. H., Wu, H. C., Tseng, C. W., Chen, S. H., n-Heptanehydroconversion on platinum-loaded mordenite and beta zeolites: The effect of reaction pressure. Applied Catalysis, A: General, 203, 211-220 (2000).

Fraenkel, D., Cherniavsky M., Ittah B., Levy M., Shape selective alkylation of naphthalene and methylnaphthalene with methanol over HZSM-5 zeolite catalysts. Journal of Catalysis, 101(2), 273-283 (1986).

Fang, Y. M., Hu, H. Q., Shape-selectivity in 2,6-dimethylnaphthalene synthesis over ZSM-5: Computational analysis using density functional theory. Catalysis Communications, 7, 264-267 (2006).

Garces, J. M., Stone, F. C., Bates, S. I., Deactivation and Regeneration of Zeolite CsNaX Catalyst Used for the Side Chain Alkylation of Toluene with Methanol. The Netherlands: Elsevier: Innovation in Zeolites Materials Science, 505-511 (1988).

Han, L., Liu, Y. X., Subhan, F., Liu, X. M., Yan, Z. F., Particle effect of SAPO-11 promoter on isomerization reaction in FCC units. Microporous and Mesoporous Materials, 194, 90-96 (2014).

Harris, J. W., Cordon, M. J., Di Iorio, J. R., Vega-Vila, J. C., Ribeiro, F. H., Gounder, R., Titration and quantification of open and closed Lewis acid sites in Sn-Beta zeolites that catalyze glucose isomerization. Journal of Catalysis, 335, 141-154 (2016).

Jin, L. J., Hu, H. Q., Wang, X. Y., Liu, C., Methylation of 2-methylnaphthalene with methanol to 2,6-dimethylnaphthalene over ZSM-5 modified by Zr an Si. Industrial & Engineering Chemistry Research, 45, 3531-3536 (2006).

Jin, L. J., Zhou, X. J., Hu, H. Q., Synthesis of 2,6-dimethylnaphthalene by methylationof 2-methylnaphthalene on mesoporous ZSM-5 by desilication. Catalysis Communications, 10, 336-340 (2008).

Lok, B. M., Messina, C. A., Patton, R. L., Gajek, R. T., Cannan, T. R., Flanigen, E. M., silicoaluminophosphates. U.S. Patent 4440871 (1984).

Liu, M., Wu, W., Kikhtyanin, O. V., Xiao, L. F., Toktarev, A. V., Wang, G. L., Zhao, A. J., Smirnova, M. Y., Echevsky, G. V., Alkylation of naphthalene with methanol over SAPO-11 molecular sieve synthesized by different crystallization methods. Microporous and Mesoporous Materials, 181, 132-140 (2013).

Liu, Y., Yan, A. Z., Xu, Q. H., Acidity, diffusion and catalytic properties of the silicoaluminophosphate SAPO-11. Applied Catalysis, A: General, 67, 169-177 (1991).

Liu, Z., Liu, L. Song, H., Wang, C., Xing, W., Komarneni, S., Yan, Z., Hierarchical SAPO-11 preparation in the presence of glucose. Materials Letters, 154, 116-119 (2015).

Lillwitz, L. D., Production of dimethyl-2,6-naphthalenedicarboxylate:precursor to polyethylene naphthalate. Applied Catalysis, A: General, 221, 337-358 (2001).

Lucas, N., Bordoloi, A., Amrute, A. P., Kasinathan, P., Vinu, A., Bohringer, W., Fletcher, J. C. Q., Halligudi, S. B., A comparative study on liquid phase alkylation of 2-methylnaphthalene with long chain olefins using different solid acid catalysts. Applied Catalysis, A: General, 352, 74-80 (2009).

Nieminen, V., Kumar, N., Heikkilä, T., Laine, E., Villegas, J., Salmi, T., Murzin, D. Y., Isomerization of 1-butene over SAPO-11 catalysts synthesized by varying synthesis time and silica sources. Applied Catalysis, A: General, 259, 227-234 (2004).

Park, J. N., Wang, J., Lee, C. W., Park, S. E., Methylation of naphthalene with methanol over beta, mordernite, ZSM-12 and MCM-22 zeolite catalysts. Bulletin of the Korean Chemical Society, 23, 1011-1013 (2002).

Prakash, A. M., Chilukuri, S. V. V., Bagwe, R. P., Ashtekar, S., Chakrabarty, D. K., Silicoaluminophosphate molecular sieves SAPO-11, SAPO-31 and SAPO-41: Synthesis, characterization and alkylation of toluene with methanol. Microporous Materials, 6, 89-97 (1996).

Pu, S. B., Inui, T., Synthesis of 2,6-dimethylnaphthalene by methylation of methylnaphthalene on various medium and large-pore zeolite catalysts. Applied Catalysis, A: General, 146, 305-316 (1996).

Rabaev, M., Landau, M. V., Vidruk-Nehemya, R., Goldbourt, A., Herskowitz, M., Improvement of hydrothermal stability of Pt/SAPO-11 catalyst in hydrodeoxygenation–isomerization–aromatization of vegetable oil. Journal of Catalysis, 332, 164-176 (2015).

Sing, K. S. W., Everett, D. H., Haul, R. A. W., Moscou, L., Pierotti, J., Rouquerol, J., Siemieniewska, T., Reporting physisorption data for gas/solid systems with special reference to the determination of surface area and porosity. Pure and Applied Chemistry, 57, 603-619 (1985).

Smith, K., Al-Khalaf, A. K. H., El-Hiti, G. A., Pattisson, S., Highly regioselective di-tert-amylation of naphthalene over reusable H-mordenite zeolite. Green Chemistry, 14, 1103-1110 (2012).

Smith, K., Roberts, S. D., Regioselective dialkylation of naphthalene. Catalysis Today, 60, 227-233 (2000).

Smith, K., Roberts, S. D., El-Hiti, G. A., Study of regioselective dialkylation of naphthalene in the presence of reusable zeolite catalysts. Organic & Biomolecular Chemistry, 1, 1552-1559 (2003).

Song, C. S., Shape-selective isopropylation of naphthalene over H-mordenite catalysts for environmentally friendly synthesis of 2,6-dialkylnaphthalene. Surface Chemistry and Catalysis: Chimie des Surfaces et Catalyse, 3, 477-496 (2000).

Song, C. S., Schobert, H. H., Opportunities for developing specialty chemicals and advanced materials from coals. Fuel Processing Technology, 34, 157-196 (1993).

Subramanian, S., Mitra, A., Satyanarayana, C. V. V., Chakrabarty, D. K., Para-selective butylation of phenol over silicoaluminophosphate molecular sieve SAPO-11 catalyst. Applied Catalysis, A: General, 159, 229-240 (1997).

Sugi, Y., Maekawa, H., Hasegawa, Y., Naiki, H., Komura, K., Kubota, Y., The alkylation of naphthalene over three-dimensional large pore zeolites: The influence of zeolite structure and alkylating agent on the selectivity for dialkylnaphthalenes. Catalysis Today, 132, 27-37 (2008).

Tian, S. S., Chen, J. X., Hydroisomerization of n-dodecane on a new kind of bifunctional catalyst: Nickel phosphide supported on SAPO-11 molecular sieve. Fuel Processing Technology, 122, 120-128 (2014).

Tsutsui, T., Ijichi, K., Inomata, T., Enhancement of conversion and selectivity by temperature-swing unsteady-state reaction method in shape-selective methylation of methylnaphthalene with ZSM-5. Chemical Engineering Science, 59, 3993-3999 (2004).

Wang, F., Luo, M., Xiao, W. D., Cheng, X. W., Long, Y. C., Coking behavior of a submicron MFI catalyst during ethanol dehydration to ethylene in a pilot-scale fixed-bed reactor. Applied Catalysis, A: General, 393, 161-170 (2011).

Wang, J. B., Li, J. Z., Xu, S. T., Zhi, Y. C., Wei, Y. X., He, Y. L., Chen, J. R., Zhang, M. Z., Wang, Q. Y., Zhang, W. N., Wu, X. Q., Guo, X. W., Liu, Z. M., Methanol to hydrocarbons reaction over HZSM-22 and SAPO-11: Effect of catalyst acid strength on reaction and deactivation mechanism. Chinese Journal of Catalysis, 36, 1392-1402 (2015).

Wang, X. X., Wen, J., Zhang, W., Zhao, L. F., Wei, W., Synthesis of 2,6-dimethyl naphthalene over SAPO-11 zeolite. Petrochemical Technology, 41, 1282-1287 (2012).

Wang, X. X., Zhang, W., Guo, S. Q., Zhao, L. F., Xiang, H. W., Optimization of the synthesis of SAPO-11 for the methylation of naphthalene with methanol by varying templates and template content. Journal of the Brazilian Chemical Society, 24, 1180-1187 (2013).

Wang, X. X., Liu Z. M., Wen, J., Zhang, W., Zhao, L. F., Study on catalytic synthesis of 2,6-dimethylnaphthalene over SAPO-11 zeolites modified by steam. Journal of Molecular Catalysis, (China), 29, 331-338 (2015).

Wei, X. L., Lu, X. H., Zhang, T. J., Chu, X., Zhou, D., Nie, R. F., Xia, Q. H., Synthesis and catalytic application of SAPO-5 by dry-gel conversion for the epoxidation of styrene with air. Microporous and Mesoporous Materials, 214, 80-87 (2015).

Wu, K., Xue, F. F., Preparation and properties of polyethylene naphthalate industrial filament fiber. China Rubber Industry, 62, 91-94 (2015).

Wu, Q. Y., Oduro, I. N., Huang, Y., Fang, Y. M., Synthesis of hierarchical SAPO-11 via seeded crystallization. Microporous and Mesoporous Materials, 218, 24-32 (2015).

Wu, W., Wu, W. G., Kikhtyanin, O. V., Li, L. F., Toktarev, A. V., Ayupov, A. B., Khabibulin, J. F., Echevsky, G. V., Huang, J., Methylation of naphthalene on MTW-type zeolites. Influence of template origin and substitution of Al by Ga. Applied Catalysis, A: General, 375, 279-288 (2010).

Yoo, K., Burckle, E. C., Smirniotis, P. G., Isobutane/2-butene alkylation using large-pore zeolites: Influence of pore structure on activity and selectivity. Journal of Catalysis, 211, 6-18 (2002).

Zhang, S. Z., Chen, S. L., Dong, P., Yuan, G. M., Xu, K. Q., Characterization and hydroisomerization performance of SAPO-11 molecular sieves synthesized indifferent media. Applied Catalysis, A: General, 332, 46-55 (2007).

Zhang, S. Z., Chen, S. L., Dong, P., Synthesis, characterization and hydroisomerization performance of SAPO-11 molecular sieves with caverns by polymer spheres. Catalysis Letters, 136, 126-133 (2010).

Zhu, S. Y., Liang, S. J., Wang, Y., Zhang X. Y., Li, F. Y., Lin, H. X., Zhang, Z. Z., Wang, X. X., Ultrathin nanosheets of molecular sieve SAPO-5: A new photocatalyst for efficient photocatalytic reduction of CO_2 with H_2O to methane. Applied Catalysis, B: Environmental, 187, 11-18 (2016).

Zhu, Z. R., Chen, Q. L., Xie, Z. K., Yang, W. M., Li, C., The roles of acidity and structure of zeolite for catalyzing toluene alkylation with methanol to xylene. Microporous and Mesoporous Materials, 88, 16-21 (2006).